




# Brain microstructural alterations in type 2 diabetes: diffusion kurtosis imaging provides added value to diffusion tensor imaging

Ying Xiong<sup>1</sup> · Yi Sui<sup>2,3</sup> · Shun Zhang<sup>1</sup> · Xiaohong Joe Zhou<sup>2,3</sup> · Shaolin Yang<sup>3,4</sup> · Yang Fan<sup>5</sup> · Qiang Zhang<sup>6</sup> · Wenzhen Zhu<sup>1</sup> 

Received: 24 May 2018 / Revised: 3 August 2018 / Accepted: 10 September 2018 / Published online: 18 October 2018  
© European Society of Radiology 2018

## Abstract

**Objectives** To investigate brain microstructural changes in white matter and gray matter of type 2 diabetes mellitus (T2DM) patients using diffusion kurtosis imaging.

**Methods** Diffusion kurtosis imaging ( $b$  values = 0, 1250, and 2500 s/mm<sup>2</sup>) was performed for 30 T2DM patients and 28 controls. FMRIB Software Library with tract-based spatial statistics was used to analyze intergroup differences in fractional anisotropy (FA), mean diffusivity (MD), mean kurtosis (MK), axial kurtosis ( $K_{\parallel}$ ), and radial kurtosis ( $K_{\perp}$ ) of multiple white matter regions. Atlas-based ROI analysis was conducted in gray matter structures and some fiber tracts. Correlations between MK changes and clinical measurements were determined.

**Results** In whole-brain tract-based spatial statistics analysis, T2DM patients exhibited abnormalities in 29.6%, 30.4%, 35.4%, 10.5%, and 26.0% of white matter regions as measured by FA, MD, MK,  $K_{\parallel}$ , and  $K_{\perp}$ , respectively, when compared to the controls. MK reduction was contributed more by the decreased  $K_{\perp}$ . In atlas-based analysis, MK detected more ROIs (27/48) with white matter microstructural changes than FA (13/48) and MD (17/48). MK decreased in bilateral thalamus and caudate, while FA showed statistically significant difference only in the left caudate. MK values negatively correlated with disease duration in the genu of corpus callosum and anterior corona radiata ( $R = -0.512$  and  $-0.459$ ) and positively correlated with neuropsychological scores in the cingulum (hippocampus) ( $R = 0.466$  and  $0.440$ ).

**Conclusions** Diffusion kurtosis imaging detects more brain regions with white matter and gray matter microstructural alterations of T2DM patients than DTI metrics. It provides valuable information for studying the pathology of diabetic encephalopathy and may lead to better imaging biomarkers for monitoring disease progression.

## Key Points

- Diffusion kurtosis imaging detects more brain regions with microstructural alterations in white matter and gray matter of T2DM patients than DTI.
- Mean kurtosis changes are associated with disease severity and impaired neuropsychological function in T2DM.
- Diffusion kurtosis imaging demonstrates potential to assess cognitive impairment in T2DM patients and predict disease progression.

**Keywords** Type 2 diabetes mellitus · Diffusion kurtosis imaging · Diffusion tensor imaging · White matter · Gray matter

✉ Qiang Zhang  
zhangqiang\_glia@126.com

✉ Wenzhen Zhu  
zhuwenzhen8612@163.com

<sup>1</sup> Department of Radiology, Tongji Hospital, Tongji Medical College, Huazhong University of Science and Technology, 1095 Jiefang Ave, Wuhan 430030, People's Republic of China

<sup>2</sup> Center for Magnetic Resonance Research, University of Illinois at Chicago, Chicago, IL, USA

<sup>3</sup> Department of Bioengineering, University of Illinois at Chicago, Chicago, IL, USA

<sup>4</sup> Department of Psychiatry, University of Illinois at Chicago, Chicago, IL, USA

<sup>5</sup> GE Healthcare, Beijing, People's Republic of China

<sup>6</sup> Department of Neurology, Tongji Hospital, Tongji Medical College, Huazhong University of Science and Technology, 1095 Jiefang Ave, Wuhan 430030, People's Republic of China

## Abbreviations

DKI	Diffusion kurtosis imaging
DTI	Diffusion tensor imaging
FA	Fractional anisotropy
FSL	Version 5.0 FMRIB Software Library
HbA1c	Glycosylated hemoglobin A1c
HC	Healthy control
MK	Mean kurtosis
MMSE	Mini-Mental State Examination
MoCA	Montreal Cognitive Assessment
ROI	Region of interest
T2DM	Type 2 diabetes mellitus
TBSS	Tract-based spatial statistics

## Introduction

Type 2 diabetes mellitus (T2DM) is a prevalent disease that affected more than 380 million people worldwide in 2014, and the number of the cases is projected to rise to 592 million by 2035 [1]. The sustained hyperglycemia can affect many organs. Brain damage caused by diabetes, in particular, has attracted increased attention in recent years [2]. Diabetic encephalopathy has been studied intensively in attempts to define the underlying neurophysiological and structural changes, together with the resultant alterations in cognitive function. Patients with T2DM reportedly have a 20–70% greater decline in cognitive performance and a 60% higher risk of developing dementia, compared with the general population [3].

It is believed that the cognition decline in diabetes is related to functional abnormalities of the brain. Thus, numerous neuroimaging studies have investigated the mechanism of diabetic encephalopathy, including cognitive impairment. For instance, Cui identified decreased spontaneous neural activities in the cingulate gyrus and bilateral thalamus/caudate [4], and dissociation pattern in the default-mode network in T2DM patients [5]. Altered functional connectivity of the thalamus has been detected in the middle temporal gyrus and other cortex regions [6]. These changes were correlated with impaired cognitive performance. Usually, functional abnormalities are considered to result from dysfunction of neurons and fiber tracts, which can also cause structural abnormalities. Reduction in total white matter, gray matter, and hippocampal volumes has been reported in T2DM patients [7, 8] using voxel-based morphometry. Also, white matter lesions have been thought to contribute to diabetic cognitive dysfunction [9]. Magnetization transfer imaging studies revealed compromised macromolecular protein pools in key fronto-striato-thalamic circuits in T2DM [10]. The impaired biophysical integrity of these macromolecular protein pools, which consist of myelin, cell membrane proteins, and phospholipids, contributes significantly to cognitive deficits.

Diffusion tensor imaging (DTI) is a non-invasive magnetic resonance imaging (MRI) technique that has been used to investigate white matter abnormalities. Based on DWI images acquired with various diffusion gradient directions, a diffusion tensor can be reconstructed. The tensor model derives parameters, including fractional anisotropy (FA), mean diffusivity (MD), and three eigenvalues, from which fiber integrity and myelination can be inferred [11]. In T2DM patients, decreased FA and increased MD, indicating widespread white matter disruptions, have been reported [12–14]. Importantly, the traditional DWI theory and DTI model assume a Gaussian distribution of water diffusion processes, leading to a mono-exponential signal decay, with increasing  $b$  values. However, the molecular diffusion of water in biological tissues often shows a non-Gaussian distribution because of restrictions imposed by diffusion barriers such as cellular membranes and intracellular organelles. To quantify the non-Gaussian property, diffusion kurtosis imaging (DKI) was developed [15]. Kurtosis metrics, including mean kurtosis (MK), axial kurtosis ( $K_{\parallel}$ ), and radial kurtosis ( $K_{\perp}$ ), have been put forth in addition to tensor model-derived metrics. These metrics can measure the complexities of structures (determined by the glial activity, reactive astrogliosis, density of neuron, synapse and neurites, and integrity of myelinated axons) [16, 17] and can be used to assess white matter and gray matter [15, 18]. In addition, DKI has been effective for monitoring microstructural changes, even within the crossing fibers [19], and has been widely applied in neurodegenerative diseases, such as Parkinson's disease [20, 21] and Alzheimer's disease [22, 23]. However, no investigation of structural abnormalities in the white matter and gray matter of T2DM patients using DKI has been reported.

The aims of this study were the following: (i) to assess changes in white matter of T2DM subjects using DKI, as well as in the thalamus, caudate, globus pallidus, and putamen, which were included as representatives of gray matter, given their important role in functional alteration in previous studies; (ii) to investigate whether DKI diffusion and kurtosis metrics could provide additional information about microstructural changes compared to DTI; and (iii) to evaluate potential associations between the microstructural alterations, measured by DKI metrics, and clinical data.

## Materials and methods

### Subjects

With approval of the Institutional Review Board, we enrolled 60 right-handed adult subjects in this prospective study. Exclusion criteria were as follows: (a) lesions in the brain, such as tumors, cerebral infarction, hemorrhage, or vascular malformation; (b) history of stroke, epilepsy, head trauma, or

brain surgical operation; (c) systemic organic disease or history of tumors; (d) diabetes other than T2DM. Among the 60 subjects, 30 were consecutive T2DM patients ( $60.6 \pm 6.01$  years; 17 females) recruited from the endocrinology clinical service of the performing hospital; this group is referred to hereafter as the DM group. Clinical examinations and laboratory tests, including blood biochemistry, plasma glucose, glycosylated hemoglobin A1c (HbA1c), and body mass index (BMI), were performed. Four T2DM subjects with very mild complications (retinopathy and nephropathy) were not excluded. The diagnosis of T2DM was based on American Diabetes Association recommendations [24].

Thirty euglycemic subjects ( $58.5 \pm 6.22$  years; 18 females), without family history of diabetes, whose fasting glucose was  $< 7.0$  mmol/L and HbA1c  $< 6.0\%$ , were recruited from the general population and enrolled as age-, gender-, and education-matched healthy controls (denoted hereafter as the HC group). Consistency in age, gender, education years, BMI, and blood biochemistry level between the DM and HC groups was determined statistically with a two-tailed Student's *t* test and a chi-square test.

### Cognitive assessment

All participants underwent comprehensive physical, neurological, and neuropsychological assessments, which included Mini-Mental State Examination (MMSE), Montreal Cognitive Assessment (MoCA), Hachinski test, Activity of Daily Living test, and Auditory Verbal Learning Test. The MMSE and MoCA cover general mental status and cognitive domains including orientation, immediate memory, delayed memory, attention/calculation, and linguistic capacity. The Auditory Verbal Learning Test and Activity of Daily Living tests were used as supplementary tests to evaluate daily life abilities and verbal memory, and the Hachinski test was used to exclude vascular dementia ( $n = 0$ ).

### Image acquisition

Images were acquired on a 3-T MRI scanner (Discovery MR750, GE Healthcare, Waukesha, WI, USA) equipped with a 32-channel head coil. High-resolution anatomical images were obtained with axial T2-weighted fluid-attenuated inversion recovery and sagittal T1-weighted three-dimensional brain volume imaging sequences to identify lesions specified in the exclusion criteria. After these acquisitions, DKI data were obtained using a dual-spin-echo echo-planar imaging sequence with two pairs of bipolar diffusion gradient pulses. The diffusion time was 20 ms. The standard SENSE-type parallel imaging technique (Array coil Spatial Sensitivity Encoding Technique) was used with an acceleration factor of 2 along phase encoding direction. Fat suppression was achieved by using a spectral-spatial excitation

pulse. Parameters were as follows: repetition time = 5000 ms; echo time = 98 ms; field of view =  $24 \times 24$  cm<sup>2</sup>; matrix size =  $128 \times 128$ ; slice thickness = 4 mm; slice number = 46 (for whole-brain coverage); *b* values = 0, 1250, and 2500 s/mm<sup>2</sup>; 25 diffusion encoding directions for each non-zero *b* value; and scan time 5 min and 45 s.

### DKI post-processing and image analysis

Two control subjects were excluded from data analysis because of excessive head movement during the scan. Three authors (Y.X., Y.S., and S.Z. with 6 years, 8 years, and 5 years of diffusion imaging experience, respectively) executed and read the images. DKI post-processing was performed with a Diffusional Kurtosis Estimator software package [25] (<http://nitrc.org/projects/dke>). DKI parametric maps (MK,  $K_{\parallel}$ , and  $K_{\perp}$ ) were obtained by fitting the diffusion MRI signal measurements to the DKI signal model, voxel-by-voxel, with a constrained weighted linear least-squares fitting algorithm using all three *b* values [25]. The diffusion tensor parameters (FA and MD) were obtained using only two *b* values (0 and 1250 s/mm<sup>2</sup>) simultaneously with the kurtosis parameters.

Version 5.0 FMRIB Software Library (FSL) (Functional Magnetic Resonance Imaging of the Brain Software Library, <http://www.fmrib.ox.ac.uk/fsl>) [26] was applied to the pre-processed diffusion kurtosis images. Voxel-wise statistical analysis of the images was performed by using tract-based spatial statistics (TBSS) [27]. After brain extraction, the “Eddy” tool was applied to correct image distortion caused by eddy current. The FA images from all subjects were aligned to an FMRIB58 FA standard space template through nonlinear co-registration. The aligned FA maps were averaged to produce a group-mean image and generate an FA skeleton highlighting the main tracts common to the whole group. For each subject, an FA threshold of 0.2 was used before projecting the aligned FA map onto this skeleton. The resulting skeletonized FA maps were then fed into a voxel-wise group-level analysis [27]. The TBSS were also applied to the other non-FA images, i.e., MD, MK,  $K_{\parallel}$ , and  $K_{\perp}$ , by using the same nonlinear warps and skeleton projection. The between-group differences of these metrics were assessed with an FSL permutation test (Randomize Tool, 500 permutations). The TBSS analysis process for FA and non-FA images was conducted strictly following the TBSS UserGuide (<https://fsl.fmrib.ox.ac.uk/fsl/fslwiki/TBSS/UserGuide>). A statistical significance level was set as  $p < 0.05$  (with family-wise error correction).

### ROI-based quantitative analysis

The Johns Hopkins University white matter tractography atlas in FSL was used as a white matter parcellation

template. The entire white matter was parceled into 48 ROIs, using Johns Hopkins University-ICBM-labels-1mm (Fig. 1a). FA, MD, MK,  $K_{\parallel}$ , and  $K_{\perp}$  were calculated separately by averaging the pixel values in each ROI (left and right) and reported as mean  $\pm$  standard deviation. A false discovery rate correction was applied for multiple comparisons. In addition to the fiber tracts in white matter, several gray matter nuclei were included because of their important function and relatively regular shape. FA and MK parameter maps were co-registered via voxel-based nonlinear registration method in Montreal Neurological Institute space. Eight gray matter nuclei templates, including all voxels of the bilateral thalamus, caudate, globus pallidus, and putamen (Fig. 1b), were extracted from anatomically labeled templates by using Rest-State fMRIData Analysis Toolkit, v.1.1, <http://www.restfmri.net> (REST). The mean values of each nucleus from DKI index maps were estimated with REST. On the basis of these values, the two groups were compared by using a two-tailed Student's *t* test with a statistical significance set at  $p < 0.05$ .

### Correlation between DKI metrics and clinical data

To gain insights into the possible relationships between DKI metric changes and clinical findings, we performed multiple linear regression analyses to evaluate the correlation of the ROI-based MK values of specific fiber tracts in the corona radiata, corpus callosum, internal/external capsule, and cingulum regions with disease duration, HbA1c level, and neuropsychological assessment scores for all 30 T2DM patients, with age and gender as the covariates. The correlation coefficient *R* and *p* values were calculated, with a statistical significance set at  $p < 0.05$ , using SPSS 17.0 software (IBM, Armonk, NY).

## Results

### Demographics and clinical measurements

The demographic, clinical, and neuropsychological data for the DM and HC groups are shown in Table 1. No significant between-group differences were observed in age, gender, BMI, or years of education. As expected, the DM group had higher values of HbA1c ( $p < 0.001$ ) and fasting and postprandial glucose ( $p < 0.001$ ) than controls. The cognitive function, evaluated by the neuropsychological tests, was significantly poorer in the DM group ( $p < 0.05$ ).

### Whole-brain white matter changes and comparisons

Figure 2 shows the parametric maps of MK,  $K_{\parallel}$ , and  $K_{\perp}$  from a T2DM subject. The whole-brain TBSS analysis revealed that 29.6% (40,788/137,832 voxels), 30.4% (41,968/137,832 voxels), 35.4% (48,832/137,832 voxels), 10.5% (14,536/137,832 voxels), and 26.0% (35,810/137,832 voxels) of parcellated white matter regions exhibited decreased FA, MD, MK,  $K_{\parallel}$ , and  $K_{\perp}$  values, respectively, for the DM group compared with these metrics in the HC group (Fig. 3) ( $p < 0.05$ , with family-wise error correction). A detailed analysis illustrated that the reduced MK in the DM group was contributed more by a decreased  $K_{\perp}$ , than did a decreased  $K_{\parallel}$ .

### ROI-based quantitative analysis

In the entire 48 white matter ROIs, according to the Johns Hopkins University-ICBM-labels-1mm atlas, more regions (27/48) had decreased MK values than decreased FA values (13/48 regions) and increased MD (17/48) in the DM group (Table 2). For example, significantly decreased FA and MK were observed in the anterior corona radiata, superior corona

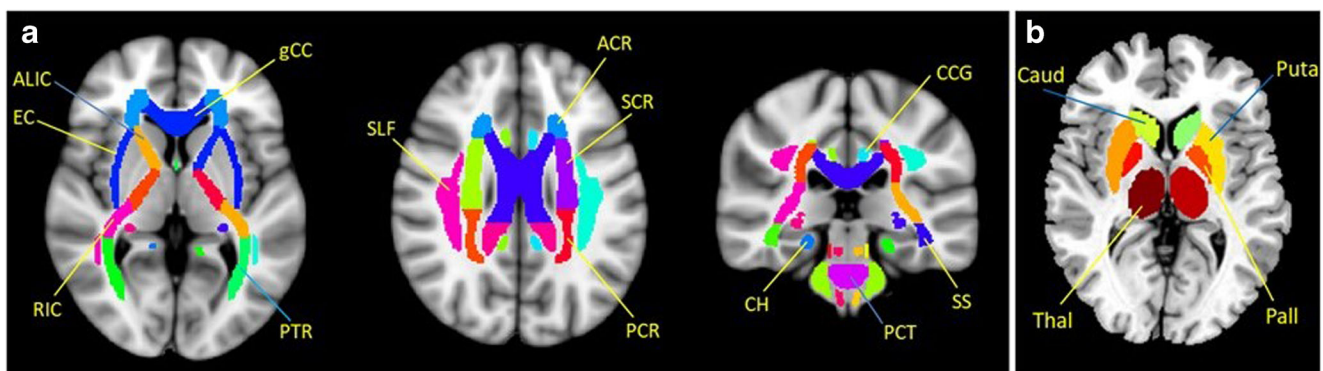


**Fig. 1** Selected ROIs in the individual fiber analysis according to the Johns Hopkins University-ICBM-labels-1mm template (a) and eight gray matter nuclei (b). Abbreviations of the white matter tracts: ALIC, anterior limb of internal capsule; EC, external capsule; RIC, retrolenticular part of internal capsule; gCC, genu of the corpus callosum; PTR, posterior

thalamic radiation; SLF, superior longitudinal fasciculus; A/S/PCR, anterior/superior/posterior corona radiata; CH, cingulum (hippocampus); PCT, pontine crossing tract; CCG, cingulum (cingulate gyrus); SS, sagittal stratum; Thal, thalamus; Puta, putamen; Pall, globus pallidus; Cau, caudate

**Table 1** Demographic data of the study groups (data are expressed as mean  $\pm$  SD or percentage number (%)) unless otherwise indicated

Clinic information	T2DM ( $n = 30$ )	HC ( $n = 28$ )	$T/\chi^2$ value	$p$ value <sup>a</sup>
Gender (female:male)	17:13	18:10	0.351	0.553 <sup>#</sup>
Age (year)	60.63 $\pm$ 6.01	58.54 $\pm$ 6.22	-1.305	0.197
Formal education (year)	11.57 $\pm$ 3.23	10.64 $\pm$ 3.35	-1.069	0.290
Hypertension <sup>b</sup>	5 (16.7)	3 (10.7)	0.432	0.511 <sup>#</sup>
Hyperlipidemia <sup>c</sup>	4 (13.3)	3 (10.7)	0.094	0.760 <sup>#</sup>
BMI ( $\text{kg}/\text{m}^2$ )	23.60 $\pm$ 3.19	24.17 $\pm$ 2.02	0.800	0.427
Diabetes duration (year)	7.49 $\pm$ 7.31	–	–	–
Insulin use	4 (13.3)	–	–	–
HbA1c (%)	7.53 $\pm$ 1.59	5.37 $\pm$ 0.40	-6.942	< 0.001
HbA1c (mmol/mol)	58.68 $\pm$ 17.45	35.23 $\pm$ 4.36	-6.909	< 0.001
Fasting glucose (mmol/L)	9.67 $\pm$ 2.63	5.20 $\pm$ 0.67	-8.728	< 0.001
Postprandial glucose (mmol/L)	13.75 $\pm$ 4.52	8.31 $\pm$ 0.95	-6.229	< 0.001
MoCA	26.53 $\pm$ 1.76	28.42 $\pm$ 1.26	4.692	< 0.001
MMSE	26.73 $\pm$ 2.49	28.29 $\pm$ 1.05	3.054	0.003
AVLT	32.37 $\pm$ 9.19	37.75 $\pm$ 8.75	2.281	0.026
Hachinski	2.06 $\pm$ 1.05	0.75 $\pm$ 0.65	-5.710	< 0.001
ADL (Barthel index)	99.4 $\pm$ 2.51	100 $\pm$ 0	1.262	0.212

MoCA Montreal Cognitive Assessment, MMSE Mini-Mental State Examination, AVLT Auditory Verbal Learning Test, ADL Activities of Daily Living

<sup>a</sup>  $p$  values labeled with superscript number sign (#) were obtained using a Pearson chi-square test (2-sided). Other  $p$  values were obtained using a 2-tailed Student's  $t$  test between the HC and the DM groups

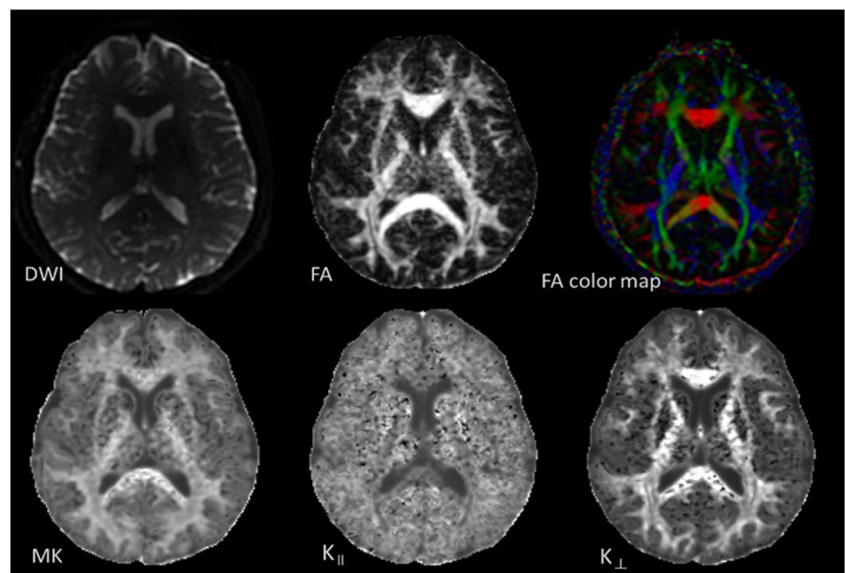
<sup>b</sup> Hypertension: systolic pressure range 140–159 mmHg or diastolic pressure ranged 90–99 mmHg. Patients with moderate and severe hypertension were excluded

<sup>c</sup> Hyperlipidemia was defined as cholesterol > 5.7 mmol/L or triglyceride > 1.7 mmol/L

radiata, and cingulum (hippocampus) in the DM group. Additionally, MK differences in the pontine crossing tract, anterior limb of internal capsule, posterior corona radiata, superior longitudinal fasciculus, and genu of corpus callosum were found. These differences are illustrated in Fig. 4a (for FA) and Fig. 4b (for MK). Figure 5 shows the box plots of

diffusion tensor and kurtosis metrics in the pontine crossing tract and posterior corona radiata [21] as examples of differences in crossing fibers between the DM and HC groups. There were no significant intergroup differences in FA and MD within the pontine crossing tract. In contrast, significant changes in MK and  $K_{\perp}$  values were detected. In posterior

**Fig. 2** Typical DKI-derived maps in a T2DM patient (female, 57 years old). DWI, diffusion-weighted imaging; FA, fractional anisotropy; MK, mean kurtosis;  $K_{\parallel}$ , axial kurtosis;  $K_{\perp}$ , radial kurtosis



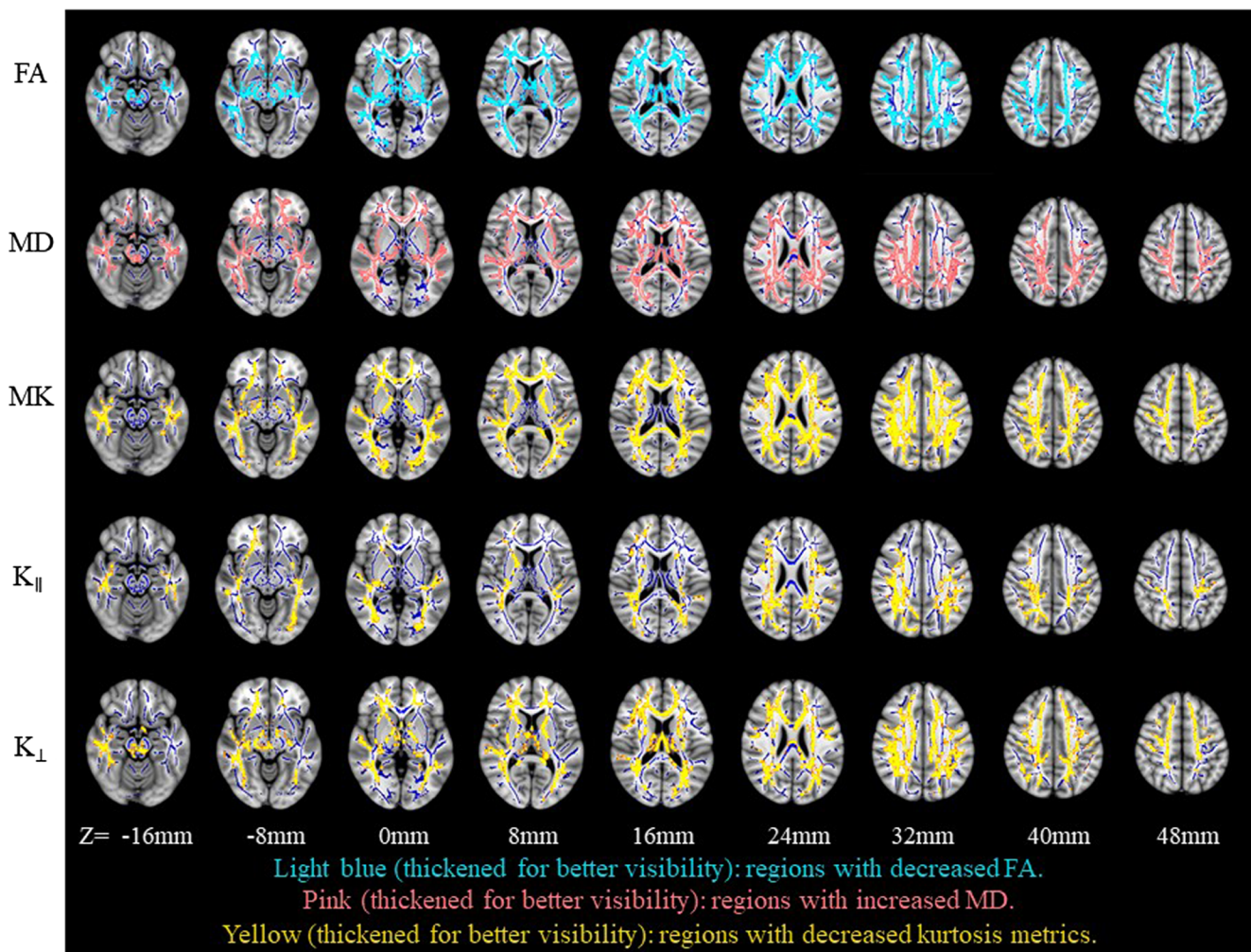


**Fig. 3** Differences in diffusion tensor metrics (FA, light blue; MD, pink) and kurtosis metrics (MK,  $K_{\parallel}$ , and  $K_{\perp}$ , yellow) between the DM and the HC groups. All results were obtained from an FSL-TBSS analysis. A

MNI152-T1-1mm-brain standard space (black and white) was used as a background image. Dark blue: FA skeleton with a threshold of 0.2 highlighting the fiber areas used in the comparison

corona radiata, every kurtosis parameter was able to detect white matter alterations while FA was not.

The MK values in bilateral thalamus and caudate of the DM group were significantly decreased compared with MK values in the HC group. However, a significant difference in FA values was present only in the left caudate (Table 3). Moreover, neither FA nor MK revealed significant intergroup differences in the bilateral putamen or globus pallidus.

### Correlation between MK values and clinical data

The correlation of the MK values of several selected fiber tracts with the clinical data revealed that MK values in the genu of corpus callosum and anterior corona radiata declined as diabetic duration increased ( $R = -0.512$  and  $-0.459$ ,  $p < 0.05$ ; Fig. 6a, b). Also, the MK values of the cingulum (hippocampus) positively correlated with the MoCA and MMSE scores ( $R = 0.466$  and  $0.440$ ,  $p < 0.05$ ; Fig. 6c, d).

MK values were not significantly correlated with the HbA1c level ( $R < 0.4$  or  $p > 0.05$ ).

### Discussion

In this study, using DKI to evaluate white matter and gray matter microstructural abnormalities in T2DM patients, we made important observations. Compared with healthy controls, T2DM patients had abnormalities, reflected by decreased FA and MK, in a variety of white matter regions, as well as in the thalamus and caudate. MK reductions occurred across a more extensive area than DTI metrics, such as in the pontine crossing tract, internal capsule, superior longitudinal fasciculus, corpus callosum, and gray matter structure. Xie [28] also characterized white matter changes in T2DM patients without cognitive impairment using DKI and voxel-based analysis. Abnormal kurtosis metrics were found in the pons and corpus callosum. There are several differences in our

**Table 2** Significant diffusion changes in the white matter tracts between T2DM patients and healthy controls during the ROI-based statistical analysis ( $p < 0.05$ , false discovery rate corrected)

Fiber tracts	FA	MD	MK	$K_{  }$	$K_{\perp}$
Corpus callosum	–	g	g, b	–	b
Anterior limb of internal capsule	–	–	Bilateral	–	Bilateral
Posterior limb of internal capsule	–	Right	Bilateral	–	–
Retrolenticular part of internal capsule	–	Bilateral	–	Right	–
Anterior corona radiata	Bilateral	Right	Bilateral	–	Bilateral
Superior corona radiata	Bilateral	–	Bilateral	–	Bilateral
Posterior corona radiata	–	Bilateral	Bilateral	Bilateral	Bilateral
Posterior thalamic radiation	–	–	–	Right	–
External capsule	Bilateral	Left	Right	–	–
Cingulum (cingulate gyrus)	Left	Left	Left	–	Left
Cingulum (hippocampus)	Bilateral	Bilateral	Bilateral	–	–
Superior longitudinal fasciculus	–	–	Bilateral	Bilateral	–
Sagittal stratum	–	Bilateral	Bilateral	Bilateral	–
Superior fronto-occipital fasciculus	Bilateral	Bilateral	–	–	Left
Uncinate fasciculus	Left	Left	Right	Right	–
Superior cerebellar peduncle	–	–	Right	–	–
Tapetum	–	–	Bilateral	–	Left
Cerebral peduncle	Right	–	–	–	–
Middle cerebellar peduncle	–	Yes	Yes	Yes	Yes
Pontine crossing tract	–	–	Yes	–	Yes
Fornix	–	–	Yes	Yes	Yes

g genu of the corpus callosum, b body of the corpus callosum

study. Since part of our T2DM subjects have cognitive impairment, we found more regions showed whiter matter alterations. Second, our investigation first included eight gray matter nuclei. Third, we compared DKI and diffusion metrics and found DKI was more sensitive in detecting changes in crossing fibers and gray matter nuclei, thus provided added value to DTI. Forth, the methodology was different. We applied whole-brain analysis (TBSS) in white matter and ROI-based quantitative analysis in both white matter and gray matter.

Clinically feasible imaging protocols (~ 5 min) have been suggested [29]. At least three  $b$  values were necessary for fitting the DKI model. Protocols with  $b$  values of 0, 1000, and 2000  $s/mm^2$  or 0, 1250, and 2500  $s/mm^2$  were frequently used in clinical studies. Since a stronger  $b$  value has the potential to probe further into intracellular space and membrane interactions [30], we considered to choose  $b$  values of 0, 1250, and 2500  $s/mm^2$  under the suggestions ( $b_1 = 0, b_2 = b_{max} - 2, b_3 = b_{max}$ , and  $b_{max} < 3000 s/mm^2$ ) [29] to characterize non-

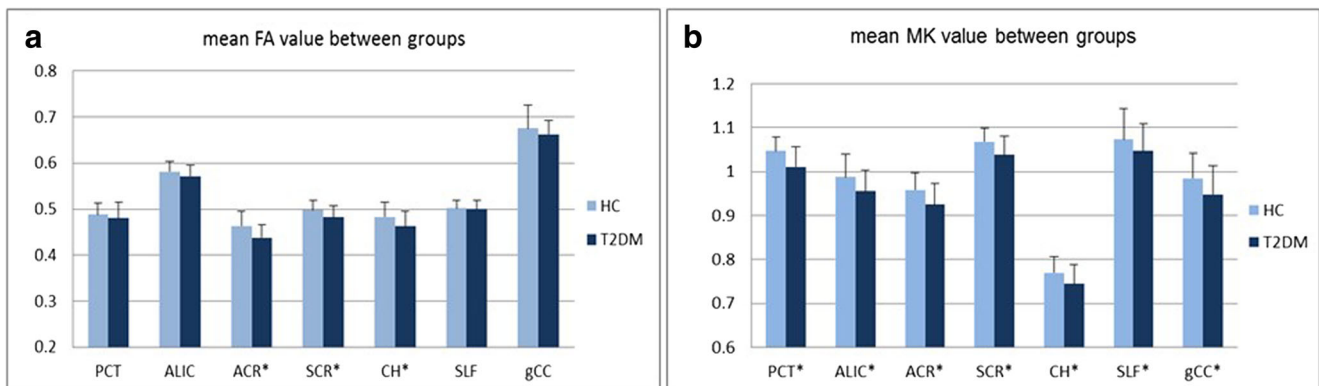


**Fig. 4** Differences in FA (a) and MK (b) values for some specific important fiber tracts in an atlas-based ROI analysis between the DM (dark) and the HC (light) groups. \*Statistically significant difference

( $p < 0.05$ ). The bar height indicates the mean, and the line on top of the bar indicates the standard deviation

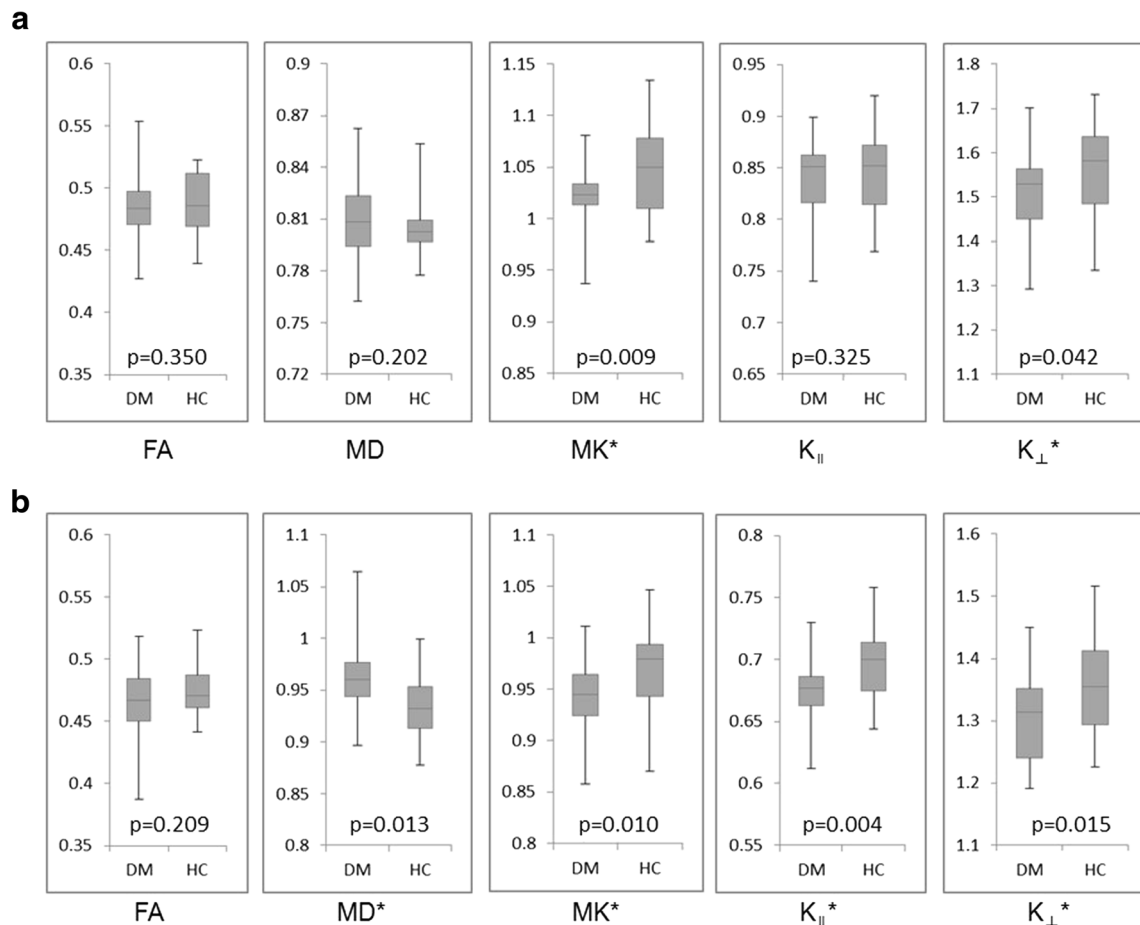


**Fig. 5** Box plots of diffusion tensor and kurtosis parameters FA, MD ( $\times 10^{-3}$  mm<sup>2</sup>/s), MK,  $K_{\parallel}$ , and  $K_{\perp}$  between the DM and HC in the pontine crossing tract (a) and posterior corona radiata (b). Boxes represent the

25th and 75th percentiles, with the median indicated by the middle line in the box. Vertical end bars denote the range of values. The asterisk (\*) indicates a significant difference ( $p < 0.05$ ) between the two groups

Gaussian diffusion process, balance the scanning time and model accuracy, and keep sufficient SNR.

Widespread white matter differences were shown in T2DM patients as indicated by FA, MD, and DKI metrics. The abnormalities in white matter that we observed from TBSS and atlas-based analyses are consistent with those of previously reported DTI findings [13, 14] and regional microstructural abnormalities in the anterior limb of the internal capsule [31], corona radiata [32], cingulum bundle [33], and superior and inferior longitudinal fasciculus [34]. These abnormalities are mostly encompassed by our observed regional abnormalities using DKI metrics. Using the global analysis method, DKI results can provide a comprehensive overview of the white matter alterations in T2DM patients.

As a feasible extension of DTI, DKI provides additional kurtosis metrics and more information regarding tissue substructure [17]. MK is defined as the average value of kurtosis over all possible gradient directions, using a plurality of  $b$  values, which is a dimensionless measure of the degree of diffusion hindrance or restriction and reflects changes in structural complexity [16, 35]. Previous studies have shown that

MK increased in brain tumors [36] because of the cellular atypia or proliferation and exuberant angiogenesis. Hybrid DK IVIM imaging can simultaneously measure cerebral perfusion and diffusion and kurtosis indexes that together improve brain tumor diagnosis [37]. As in neurodegenerative disease, MK increased in gray matter and the thalamus in Alzheimer's disease [22] and in the substantia nigra in Parkinson's disease [20]. These abnormalities were considered to be related to amyloid plaque or iron deposition. MK has been found to decrease in the thalamus and internal capsule of mild traumatic brain injury [38], in the temporal lobe of idiopathic epilepsy [39], and in some psychiatric diseases, such as depression and internet gaming addiction [40]. The reduced MK in brain is likely related to impoverished cell compartmentalization and an increase in membrane permeability [29, 41]. In our results, the decreased MK values in the DM group indicated reduced structural complexity, which is postulated to reflect axons/myelin loss in the white matter. Furthermore,  $K_{\parallel}$  and  $K_{\perp}$  measure the kurtosis along the directions parallel and perpendicular to the principal diffusion direction [16, 35]; thus, they can be used to reflect the integrity



**Table 3** ROI values of diffusion tensor and kurtosis metrics measured in bilateral caudate, pallidum, putamen, and thalamus in healthy controls and T2DM subjects

Metrics	FA value			MK value		
	T2DM	HC	<i>p</i> value	T2DM	HC	<i>p</i> value
Caudate_L	0.222 ± 0.010	0.229 ± 0.014	0.020*	0.541 ± 0.035	0.560 ± 0.031	0.039*
Caudate_R	0.229 ± 0.014	0.237 ± 0.019	0.076	0.548 ± 0.033	0.569 ± 0.037	0.022*
Pallidum_L	0.296 ± 0.015	0.299 ± 0.012	0.291	0.758 ± 0.029	0.762 ± 0.028	0.593
Pallidum_R	0.281 ± 0.011	0.282 ± 0.010	0.594	0.741 ± 0.026	0.733 ± 0.028	0.266
Putamen_L	0.288 ± 0.009	0.290 ± 0.009	0.250	0.667 ± 0.021	0.666 ± 0.018	0.811
Putamen_R	0.293 ± 0.011	0.295 ± 0.010	0.450	0.649 ± 0.023	0.649 ± 0.018	0.951
Thalamus_L	0.303 ± 0.015	0.310 ± 0.016	0.071	0.623 ± 0.036	0.642 ± 0.034	0.040*
Thalamus_R	0.317 ± 0.014	0.323 ± 0.015	0.144	0.637 ± 0.033	0.656 ± 0.034	0.036*

Data are expressed as mean ± SD. *P* values with asterisk (\*) were significantly different. All the *p* values were obtained with a 2-tailed Student’s *t* test between groups

T2DM type 2 diabetes mellitus, HC healthy controls

of axons and myelin. Quantitative analysis showed more extensive regions had reduced  $K_{\perp}$  than  $K_{\parallel}$ . Areas with  $K_{\parallel}$  difference were almost encompassed in the areas with  $K_{\perp}$  difference, except only for the white matter in the left temporal lobe and posterior thalamic radiation (Fig. 3).  $K_{\perp}$  contributed more to MK changes than did  $K_{\parallel}$  in white matter regions. Thus, we concluded that the compromise of myelin sheath is more significant than the impairment and decrement of axons.

Unlike DTI metrics, MK is not limited to anisotropic environments; hence, it especially permits quantification of the microstructural integrity in the presence of crossing fibers [19]. This characteristic may explain why DKI metrics identified more compromised white matter regions than FA in our study. DKI is also sensitive to gray matter, as the metric is not dependent on the spatial orientation of brain tissue microstructure, unlike FA and MD. The ROI analysis on bilateral

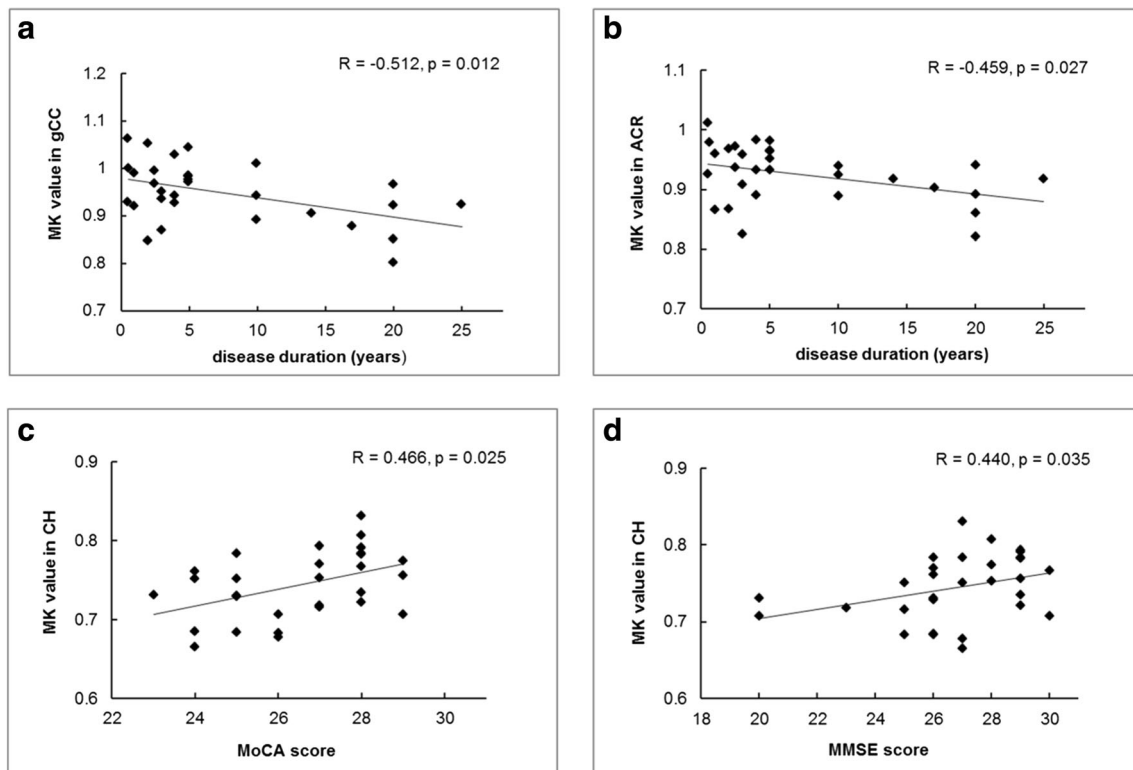


**Fig. 6** Correlation between the MK values of the genu of the corpus callosum and the anterior corona radiata with disease duration (a, b), and between the MK values of the cingulum (hippocampus) (CH) and the neuropsychological scores (c, d). The correlation was determined

using data from all 30 type 2 diabetes mellitus patients (represented by the dots). Results from linear regression are indicated in the figure (R, correlation coefficient)

thalamus and caudate also showed decreased MK in the DM group. The thalamus, one of the important gray matter nuclei near basal ganglia, is considered the sensory and movement relay station for neuron substitution between the cerebral cortex and the spinal cord [42]. These gray matter structures have a high density of neuronal soma and synapses. The involvement of thalamic nuclei in sensory systems was confirmed [42]. Thalamic nuclei are also believed to be involved in cognition, especially in familiarity and recollective processes through the mammillo-thalamic tract [43]. Furthermore, several thalamic nuclei have been demonstrated within some specific projections [44] and related to different neuronal circuits, such as fronto-striato-thalamic circuits, in which the head of the caudate nucleus also is involved [10]. The MK decline in this region might be related to neuronal loss, gliosis, and compromised synapses, which lead to reduced structural complexity. Decreased microstructure integrity in these gray matter nuclei can result in malfunction of neuronal circuits and lead to decline in cognition. The combined findings in the compromised macromolecular protein pools [10] and reduced microstructural integrity and complexity of the subcortical regions, such as the thalamus, have broad implications for the underlying neuronal circuitry of the neurological pathophysiology and underlying substrates linking T2DM and cognitive deficits. Information provided by DKI metrics can characterize subtle tissue alterations in brain quantitatively, monitor disease progression dynamically, and help predict prognosis of cognition impairment in T2DM patients. MK and  $K_{\perp}$  showed potential to be imaging biomarkers. DKI-derived metrics can also be used to evaluate the outcome of some targeted interventions, such as anti-dementia and neurotrophic agents (e.g., donepezil, rivastigmine, and gangliosides).

Our quantitative ROI analysis showed correlations between reduced MK values in the genu of the corpus callosum and anterior corona radiata and disease duration, and between increased MK value in the cingulum (hippocampus) and MoCA/MMSE scores. It is possible that white matter structural abnormalities occur and develop as the diabetes progresses. Lower scores of neuropsychological tests indicate more severe cognitive impairment, which may be caused by axon or myelin decrement and reflected by MK values in the cingulum (hippocampus) area. We found no significant correlation between MK and HbA1c values. Since the DM group had higher HbA1c values, poorer plasma glucose control maybe one of the contributors to the white matter and gray matter changes. However, HbA1c reflects the plasma glucose state in the recent 8 to 12 weeks; its level can fluctuate slightly sometimes according to the plasma glucose control situation. A longer time may be needed for the white matter alterations to develop. In addition, drug effects, individual patient differences, and hemoglobin abnormalities might affect these alterations.

This study has limitations. First, the relatively small sample size may limit generalization of the results. Second, the

correlation  $R$  value was moderate (around 0.5), so it remains to be determined if the abnormalities in some white matter regions in the T2DM brain have significant implications for the disease. More neuropsychological assessments with better specification and detailed rating scale are needed in future study. Third, we used three  $b$  values (0, 1250, 2500 s/mm<sup>2</sup>) as a clinically feasible protocol. The accuracy of these measures might improve, if six  $b$  values (0–2500 in increments of 500 s/mm<sup>2</sup>) [29] or the estimated DKI method with five  $b$  values [45] was used. However, this change cannot be made because a short scan time is essential to minimize elder patient discomfort and movement during MRI scans.

In conclusion, to the best of our knowledge, this is the first DKI study investigating both white matter and gray matter microstructural changes in T2DM patients. With both diffusion and kurtosis metrics, DKI demonstrated to provide additional information about white matter abnormalities in T2DM patients than DTI. DKI indices may better reflect decreased structural complexities in the white matter and thalamus and caudate of T2DM patients. These alterations may be caused by compromised fiber tracts and abnormal loss of neuron and synapses, with consequent decreased neuronal signal transmission. Our findings contribute to understanding the neuropathological process of diabetic encephalopathy and cognitive impairment. DKI may also lead to better imaging biomarkers for monitoring disease progression in the brain and early intervention treatment.

**Funding** This study has received funding by the National Natural Science Foundation of China (grant numbers 81601480, 81471230, and 81171308).

## Compliance with ethical standards

**Guarantor** The scientific guarantor of this publication is Wenzhen Zhu.

**Conflict of interest** The authors declare that they have no conflict of interest.

**Statistics and biometry** No complex statistical methods were necessary for this paper.

**Informed consent** Written informed consent was obtained from all subjects in this study.

**Ethical approval** Institutional Review Board approval was obtained.

**Study subjects or cohorts overlap** Some study subjects or cohorts have been previously reported in part at the 101st Annual Meeting of the Radiological Society of North America, Chicago, USA, 25–30 November 2015.

## Methodology

- prospective
- diagnostic or prognostic study
- performed at one institution

## References

- Guariguata L, Whiting DR, Hambleton I, Beagley J, Linnenkamp U, Shaw JE (2014) Global estimates of diabetes prevalence in adults for 2013 and projections for 2035. *Diabetes Res Clin Pract* 103:137–149
- Brundel M, Kappelle LJ, Biessels GJ (2014) Brain imaging in type 2 diabetes. *Eur Neuropsychopharmacol* 24:1967–1981
- Strachan MW, Price JF, Frier BM (2008) Diabetes, cognitive impairment, and dementia. *BMJ* 336(7634):6
- Cui Y, Jiao Y, Chen YC et al (2014) Altered spontaneous brain activity in type 2 diabetes: a resting-state functional MRI study. *Diabetes* 63:749–760
- Cui Y, Jiao Y, Chen HJ et al (2015) Aberrant functional connectivity of default-mode network in type 2 diabetes patients. *Eur Radiol* 25:3238–3246
- Chen YC, Xia W, Qian C, Ding J, Ju S, Teng GJ (2015) Thalamic resting-state functional connectivity: disruption in patients with type 2 diabetes. *Metab Brain Dis* 30:1227–1236
- Moran C, Phan TG, Chen J et al (2013) Brain atrophy in type 2 diabetes: regional distribution and influence on cognition. *Diabetes Care* 36:4036–4042
- Wu G, Lin L, Zhang Q, Wu J (2017) Brain gray matter changes in type 2 diabetes mellitus: a meta-analysis of whole-brain voxel-based morphometry study. *J Diabetes Complications* 31:1698–1703
- Jongen C, van der Grond J, Kappelle LJ et al (2007) Automated measurement of brain and white matter lesion volume in type 2 diabetes mellitus. *Diabetologia* 50:1509–1516
- Yang S, Ajilore O, Wu M, Lamar M, Kumar A (2015) Impaired macromolecular protein pools in fronto-striato-thalamic circuits in type 2 diabetes revealed by magnetization transfer imaging. *Diabetes* 64:183–192
- Le Bihan D, Mangin JF, Poupon C et al (2001) Diffusion tensor imaging: concepts and applications. *J Magn Reson Imaging* 13:534–546
- Hsu JL, Chen YL, Leu JG et al (2012) Microstructural white matter abnormalities in type 2 diabetes mellitus: a diffusion tensor imaging study. *Neuroimage* 59:1098–1105
- Xiong Y, Sui Y, Xu Z et al (2016) A diffusion tensor imaging study on white matter abnormalities in patients with type 2 diabetes using tract-based spatial statistics. *AJNR Am J Neuroradiol* 37:1462–1469
- Zhang J, Wang Y, Wang J et al (2014) White matter integrity disruptions associated with cognitive impairments in type 2 diabetic patients. *Diabetes* 63:3596–3605
- Hui ES, Cheung MM, Qi L, Wu EX (2008) Towards better MR characterization of neural tissues using directional diffusion kurtosis analysis. *Neuroimage* 42:122–134
- Steven AJ, Zhuo J, Melhem ER (2014) Diffusion kurtosis imaging: an emerging technique for evaluating the microstructural environment of the brain. *AJR Am J Roentgenol* 202:W26–W33
- Jensen JH, Helpem JA, Ramani A, Lu H, Kaczynski K (2005) Diffusional kurtosis imaging: the quantification of non-Gaussian water diffusion by means of magnetic resonance imaging. *Magn Reson Med* 53:1432–1440
- Cheung MM, Hui ES, Chan KC, Helpem JA, Qi L, Wu EX (2009) Does diffusion kurtosis imaging lead to better neural tissue characterization? A rodent brain maturation study. *Neuroimage* 45:386–392
- Lazar M, Jensen JH, Xuan L, Helpem JA (2008) Estimation of the orientation distribution function from diffusional kurtosis imaging. *Magn Reson Med* 60:774–781
- Wang JJ, Lin WY, Lu CS et al (2011) Parkinson disease: diagnostic utility of diffusion kurtosis imaging. *Radiology* 261:210–217
- Kamagata K, Tomiyama H, Hatano T et al (2014) A preliminary diffusional kurtosis imaging study of Parkinson disease: comparison with conventional diffusion tensor imaging. *Neuroradiology* 56:251–258
- Gong NJ, Chan CC, Leung LM, Wong CS, Dibb R, Liu C (2017) Differential microstructural and morphological abnormalities in mild cognitive impairment and Alzheimer's disease: evidence from cortical and deep gray matter. *Hum Brain Mapp* 38:2495–2508
- Falangola MF, Jensen JH, Tabesh A et al (2013) Non-Gaussian diffusion MRI assessment of brain microstructure in mild cognitive impairment and Alzheimer's disease. *Magn Reson Imaging* 31:840–846
- American Diabetes Association (2013) Diagnosis and classification of diabetes mellitus. *Diabetes Care* 36(Suppl 1):S67–S74
- Tabesh A, Jensen JH, Ardekani BA, Helpem JA (2011) Estimation of tensors and tensor-derived measures in diffusional kurtosis imaging. *Magn Reson Med* 65(3):823–836
- Jenkinson M, Beckmann CF, Behrens TEJ, Woolrich MW, Smith SM (2012) FSL. *Neuroimage* 62:782–790
- Smith SM, Johansen-Berg H, Jenkinson M et al (2007) Acquisition and voxelwise analysis of multi-subject diffusion data with tract-based spatial statistics. *Nat Protoc* 2:499–503
- Xie Y, Zhang Y, Qin W, Lu S, Ni C, Zhang Q (2017) White matter microstructural abnormalities in type 2 diabetes mellitus: a diffusional kurtosis imaging analysis. *AJNR Am J Neuroradiol* 38:617–625
- Jensen JH, Helpem JA (2010) MRI quantification of non-Gaussian water diffusion by kurtosis analysis. *NMR Biomed* 23:698–710
- Le Bihan D (2013) Apparent diffusion coefficient and beyond: what diffusion MR imaging can tell us about tissue structure. *Radiology* 268:318–322
- Zhang A, Ajilore O, Zhan L et al (2013) White matter tract integrity of anterior limb of internal capsule in major depression and type 2 diabetes. *Neuropsychopharmacology* 38:1451–1459
- Frøkjær JB, Andersen LW, Brock C et al (2013) Altered brain microstructure assessed by diffusion tensor imaging in patients with diabetes and gastrointestinal symptoms. *Diabetes Care* 36:662–668
- Hoogenboom WS, Marder TJ, Flores VL et al (2014) Cerebral white matter integrity and resting-state functional connectivity in middle-aged patients with type 2 diabetes. *Diabetes* 63:728–738
- Reijmer YD, Brundel M, de Bresser J et al (2013) Microstructural white matter abnormalities and cognitive functioning in type 2 diabetes: a diffusion tensor imaging study. *Diabetes Care* 36:137–144
- Wu EX, Cheung MM (2010) MR diffusion kurtosis imaging for neural tissue characterization. *NMR Biomed* 23:836–848
- Raab P, Hattingen E, Franz K, Zanella FE, Lanfermann H (2010) Cerebral gliomas: diffusional kurtosis imaging analysis of microstructural differences. *Radiology* 254:876–881
- Wu WC, Yang SC, Chen YF, Tseng HM, My PC (2017) Simultaneous assessment of cerebral blood volume and diffusion heterogeneity using hybrid IVIM and DK MR imaging: initial experience with brain tumors. *Eur Radiol* 27:306–314
- Grossman EJ, Ge Y, Jensen JH et al (2012) Thalamus and cognitive impairment in mild traumatic brain injury: a diffusional kurtosis imaging study. *J Neurotrauma* 29:2318–2327
- Gao J, Feng ST, Wu B et al (2015) Microstructural brain abnormalities of children of idiopathic generalized epilepsy with generalized tonic-clonic seizure: a voxel-based diffusional kurtosis imaging study. *J Magn Reson Imaging* 41:1088–1095

40. Sun Y, Sun J, Zhou Y et al (2014) Assessment of in vivo microstructure alterations in gray matter using DKI in internet gaming addiction. *Behav Brain Funct* 10:37
41. Lee CY, Bennett KM, Debbins JP (2013) Sensitivities of statistical distribution model and diffusion kurtosis model in varying microstructural environments: a Monte Carlo study. *J Magn Reson* 230: 19–26
42. Steriade M, Llinás RR (1988) The functional states of the thalamus and the associated neuronal interplay. *Physiol Rev* 68:649–742
43. Carlesimo GA, Lombardi MG, Caltagirone C (2011) Vascular thalamic amnesia: a reappraisal. *Neuropsychologia* 49:777–789
44. Hintzen A, Pelzer EA, Tittgemeyer M (2018) Thalamic interactions of cerebellum and basal ganglia. *Brain Struct Funct* 223:569–587
45. Tachibana Y, Obata T, Tsuchiya H et al (2016) Diffusion-tensor-based method for robust and practical estimation of axial and radial diffusional kurtosis. *Eur Radiol* 26:2559–2566